The missing pathway in current visuospatial processing models

Ahmad Beyh[1,2], Flavio Dell'Acqua[2], Carlo Sestieri[3], Massimo Caulo[3], Giuseppe Zappalà[4], Daniele Cancemi[1], Francisco De Santiago Requejo[1], Sergio Della Sala[5], Dominic ffytche[6], Marco Catani[1,2,†]

[1] *NatBrainLab, Department of Neuroimaging, Institute of Psychiatry, Psychology and Neuroscience, King's College London, UK*

[2] *NatBrainLab, Sackler Institute for Translational Neurodevelopment, Department of Forensic and Neurodevelopmental Science, Institute of Psychiatry, Psychology and Neuroscience, King's College London, UK*

[3] *Department of Neuroscience, Imaging and Clinical Sciences, Institute of Advanced Biomedical Technologies, University of Chieti, Italy*

[4] *Behavioral Neurology Unit, Garibaldi Hospital, Catania, Italy*

[5] *Human Cognitive Neuroscience, Psychology, University of Edinburgh, UK*

[6] *Department of Old Age Psychiatry, Institute of Psychiatry, Psychology and Neuroscience, King's College London, UK*

Summary: Spatial configuration learning depends on the parahippocampal place area (PPA), a functionally heterogenous area which current visuo-spatial processing models place downstream from parietal cortex and area V4 of early visual cortex (EVC). Here, we present evidence for the medial occipital longitudinal tract (MOLT), a novel white matter pathway connecting the PPA with EVC earlier than V4. By using multimodal imaging and neuropsychological assessments in the unique case of Patient 1, we demonstrate that an occipital stroke sparing the PPA but disconnecting the MOLT can lead to chronic deficits in configuration learning. Further, through an advanced, data-driven clustering analysis of diffusion MRI structural connectivity in a large control cohort, we demonstrate that the PPA sits at the confluence of the MOLT and the parieto-medial-temporal branch of the dual-stream model. The MOLT may therefore support multi-stage learning of object configuration by allowing direct reciprocal exchange between the PPA and EVC.

Keywords: configuration learning, visuospatial learning, parahippocampal place area, stroke, white matter, tractography, connectivity, disconnection, clustering, dual-stream model.

† Corresponding author:
Marco Catani, PO 50 IoPPN, De Crespigny Park, London SE5 8AF, UK.
m.catani@iop.kcl.ac.uk

INTRODUCTION

Configuration learning requires one to build associations between objects and their locations in the visual scene. Although the hippocampus plays a key role in spatial learning (Burgess et al., 2002; Maguire et al., 2000; O'Keefe and Dostrovsky, 1971), these object-place associations seem to rely more on the parahippocampal gyrus (PHG) (Aguirre et al., 1996; Maguire et al., 1998; Owen et al., 1996) and take place independently from hippocampal function (Bohbot et al., 1998; Maguire et al., 1998; Ploner et al., 2000). As such, configuration learning is dissociated from the memory for object identities and separate anatomical substrates have been identified for each in human (Bohbot et al., 1998, 2015; Pihlajamäki et al., 2004) and non-human primates (Malkova and Mishkin, 2003). Focal lesion studies have linked configuration memory to an area of the posterior collateral sulcus (CoS) known as the parahippocampal place area (PPA) (Bohbot et al., 1998, 2015; Epstein and Kanwisher, 1998; Ploner et al., 2000). Conversely, memory for objects has been associated with a larger number of regions distributed along the ventral visual pathway (Konen et al., 2011; Mcnaughton et al., 1989; Mishkin et al., 1983).

Based on this and other evidence of anatomical connectivity, Kravitz et al. (2011a) revised the classical dual-stream model for visuo-spatial processing (Mishkin et al., 1983) to include, within the dorsal stream for spatial processing, a branch connecting the posterior parietal lobe to the medial temporal lobe (MTL), including the hippocampus and PPA. The revised model predicts that deficits in configuration learning may derive from either parietal or selective PPA lesions and is compatible with classical neurological cases described in the literature to date (Aguirre and D'Esposito, 1999; Bohbot et al., 1998, 2015; Kravitz et al., 2011a). Indeed, the focus in recent literature has been on studying and creating computational models of parietal, retrosplenial and posterior cingulate cortex and their local and extended circuitry (Bicanski and Burgess, 2018; Boccia et al., 2017; Silson et al., 2019; van Wijngaarden et al., 2020), but less so on the sources of input to the PPA.

Evidently, the PPA occupies a central role in the spatial learning domain, particularly configuration learning. Early descriptions of the PPA focused on its preferential responses to visual stimuli depicting scenes (Epstein and Kanwisher, 1998; Epstein et al., 1999) and treated it as a single functional unit. Subsequent investigations revealed that functional responses within the PHG were organised along an anterior-to-posterior gradient, with anterior PHG being more involved in identity encoding, and responses to configuration changes occupying

more posterior locations (Pihlajamäki et al., 2004). Resting state fMRI connectivity analyses revealed a similar gradient within the PPA itself based on functional coupling to early visual cortex (EVC), parietal and frontal regions (Baldassano et al., 2013, 2016). To date, it is unclear whether this functional gradient within the PPA is driven by local, intrinsic organisation or by external anatomical input.

Here, we combine detailed clinical assessment and multimodal imaging analysis in the unique stroke case of Patient 1, and a large cohort of healthy controls to demonstrate that PPA afferent projections from EVC are necessary for configuration learning.

Patient 1 had specific impairments in configuration learning tasks following a bilateral occipital stroke. Despite a permanent reduction in his visual field due to the partial damage of his early visual cortex (EVC), the patient, a former clay target shooter competing at the national level, regained high performance at the shooting range while his memory for objects and landmarks remained intact. Extensive neuroimaging investigation, including structural, functional, and diffusion MRI, allowed us to attribute his cognitive deficit to a disconnection mechanism affecting connections between low-level EVC and the PPA.

The existence of these connections, their cortical projections and their place within the larger network of spatial learning regions were confirmed using both data-driven and manual tractography analyses of diffusion MRI data based on a large cohort of healthy participants from the Human Connectome Project (HCP, https://www.humanconnectome.org/). These analyses revealed that EVC projects to a different sub-zone of the PPA than the RSC, suggesting that the PPA contains several anatomo-functional units serving different roles in the visuo-spatial learning domain. Tractography dissections of these connections are accessible online through the MegaTrack Atlas (https://megatrackatlas.org/).

This is a unique case study describing a selective configuration learning impairment caused by a white matter disconnection following lesions outside the parietal and temporal lobes. The case highlights that the PPA receives direct inputs from low-level EVC that are indispensable for configuration learning. Our findings call for an extension of the dual-stream model to accommodate the existence of a parallel, medial visual pathway which directly supports spatial learning.

RESULTS

Patient 1: General cognitive performance

Patient 1, a right-handed male in his mid-fifties, is a construction worker and proficient clay target shooter. He was admitted to hospital in early 2015 due to sepsis where he later entered a coma. Upon regaining consciousness after 17 days, he complained of visual deficits and difficulty in remembering object locations and navigating familiar environments. Initial bedside and campimetry testing indicated that Patient 1 had a near-complete homonymous loss of the left visual hemifield and lower right quadrant secondary to bilateral occipital ischaemic lesions documented by structural brain imaging (Figure 1). At no point were any deficits observed in object naming, verbal working memory, or the recall of verbal instructions related to directions and orientation. A comprehensive testing battery performed two years post-stroke demonstrated that Patient 1 had normal general cognitive abilities (Supplemental Material).

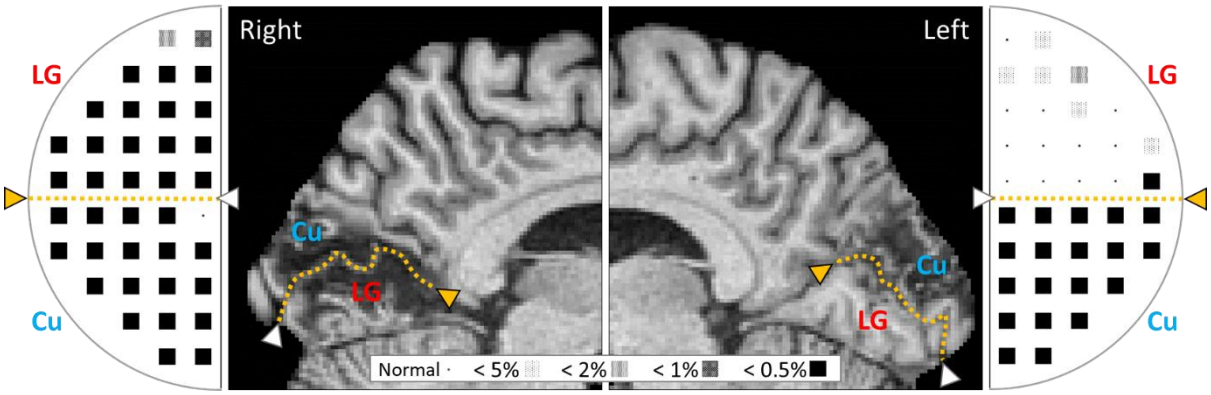

Figure 1. Lesion extent and visual deficits in Patient 1

Anatomical extent of the stroke lesion on MRI (T1weighted) and resulting visual deficit (campimetry) in Patient 1 The cuneus was severely damaged bilaterally and the lesion extended to both grey and white matter. The right lingual gyrus was also damaged but to a lesser extent while the left lingual was mostly spared except for minimal anterior damage (see also Figure S1). The lesion resulted in a near-complete homonymous loss of the left visual hemifield and lower right quadrant. The severity of the visual loss revealed by campimetry is indicated on a five-point scale: black squares in the diagrams indicate complete visual loss; the three intermediate lighter patterns indicate less severe visual loss; dots indicate normal vision. The horizontal meridian corresponds to the fundus of the calcarine sulcus (orange dotted lines). Foveal vision (centre of the visual field) corresponds to the occipital pole (white arrow heads) while peripheral vision corresponds to the anterior tip of the calcarine sulcus (orange arrow heads). LG: lingual gyrus. Cu: cuneus.

While Patient 1's visual deficits and general cognitive abilities remained stable over a period of three years, his navigation skills changed over time. Initially, when asked to draw a map of his house and neighbourhood, Patient 1 showed disorientation for cardinal points and for the layout of furniture, doors and windows in the kitchen, bedroom and living room. He also reported difficulties in recognising familiar routes and, on one occasion, he got lost while hunting. Conversely, his memory for famous landmarks (visual recognition test) and geographical locations (drawing of local streets, main towns of his region) remained intact. However, his navigation difficulties lasted for less than a year as documented by a real-world navigation task where he showed a normal ability to learn the new environment, repeat the newly learned route, and locate and name the relevant landmarks (more details in Supplemental Material).

Patient 1 resumed his clay target shooting activity and his performance recovered surprisingly well. Prior to stroke, his mean hit rate was 95%. He first returned to the shooting range 13 months after his stroke, but his performance was expectedly poor (36% hit rate). His performance gradually improved, and, by 18 months post-stroke, his hit rate was up to 80%. Although he did not fully recover his initial performance level, his recovery was remarkable given the extent of his visual deficit.

Patient 1: Specific visual configuration learning

Further assessments were performed over a period of three years post-stroke to study Patient 1's spatial configuration learning skills in detail. Patient 1's ability to identify changes in the identity or location of objects was assessed using a test adapted from Bohbot et al. (2015). In this test, Patient 1 correctly identified 90% of object identity changes, but only 50% of the spatial changes. This places him in a similar performance band as the one reported for the parahippocampal lesion group by Bohbot et al. (2015). However, this test is fast-paced and assesses the implicit learning of identities and locations as it does not ask the patient to explicitly name or locate the stimuli.

Therefore, we devised an additional test for the assessment of Patient 1's ability to simultaneously learn the identity and position of faces, letters and animals (Figure 2). In each trial, a 6x6 grid with seven stimuli that belong to the same category was presented for 5 s, after which Patient 1 was asked to indicate the position of the items on an empty grid, or verbally

recall their identities. The number of items correctly located and recalled was recorded for each trial, and the grid was presented again until all identities and locations were learned. Across the three stimulus categories, Patient 1 learned stimulus identities in 4.67±1.70 trials, while he required 19.33±1.70 trials to learn their locations. Patient 1's ability to learn identities was similar to controls (5.83±0.89 trials), whereas his configuration learning was severely impaired in comparison (5.67±0.94 trials).

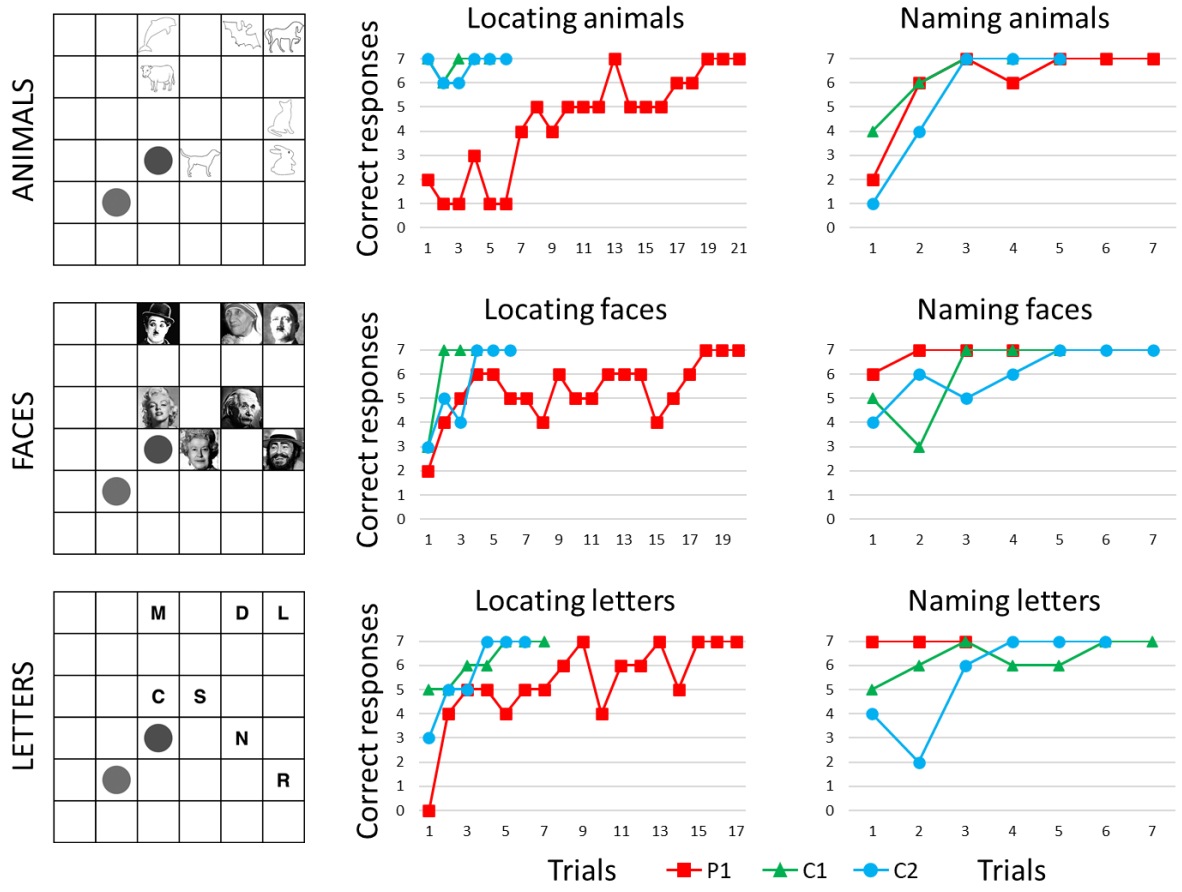

Figure 2. Specific configuration learning deficit in Patient 1

Patient 1 had impaired configuration learning with intact identity learning. The grids on the left show three different stimulus categories used to assess learning ability in Patient 1 and two controls. The grid contains seven stimuli from the given category and two disks which act as placeholders. The filled grid is shown for 5 s, then the participant is asked to either point to the stimulus locations on an empty grid, or verbally recall the stimulus identities. This is repeated until the configuration and identities are fully learned. The graphs show that Patient 1 required many more trials than controls to learn stimulus locations across all three stimulus categories, while he was indistinguishable from controls for learning stimulus identities.

Patient 1: Structural and functional extent of the lesion

Structural MRI images were used to define the lesion extent in the cortex and the underlying white matter in Patient 1 (Figure 1). The lesion severely affected the cortex and white matter of the cuneus (Cu) bilaterally, the right lingual gyrus (LG) and underlying white matter, and a small portion of the left LG and inferior-most right retrosplenial cortex (RSC). The occipital pole and the posterior-most calcarine cortex were largely spared in both hemispheres. The extent of the lesion is compatible with the campimetry results (Figure 1). In addition, a smaller lesion was located near the right inferior frontal gyrus, but it seems that this lesion did not lead to any apparent symptoms.

To define the functional extent of the lesion, Patient 1 performed a 'places vs. faces' fMRI paradigm and activation maps were compared to group average maps from a control cohort (Figure 3). Functional activations were observed in spared medial and posterior occipital tissue, corresponding to EVC, as well as an array of cortical areas outside the lesioned zone extending into temporal, retrosplenial and parietal cortex. The PPA was successfully identified bilaterally in the posterior CoS and anterior-most ventral tip of the LG as a locus of preferential responses to images of places compared to those of faces (Figure 3).

Patient 1: White matter tract analysis

Diffusion MRI was acquired from Patient 1 and tractography used to quantify the extent of white matter damage. Spherical deconvolution (SD) tractography showed severe damage to fibres leaving anterior EVC and coursing towards the MTL. The anterior terminations of these fibres were intact and overlapped the functionally defined PPA (Figure 3). In the left hemisphere, tract volume was 6.7 mL and the overall tract reconstruction yielded a dense bundle of 902 streamlines. In comparison, the right hemisphere tract volume was 4.5 mL with a much sparser bundle of only 132 streamlines. The sparsity of the bundle in the right hemisphere was confirmed with the hindrance modulated orientational anisotropy (HMOA) metric, which is a surrogate for fibre density (Dell'Acqua and Tournier, 2019; Dell'Acqua et al., 2013). Left hemisphere HMOA was 0.0079 ± 0.0036, while it was lower at 0.0054 ± 0.0017

in the right hemisphere. Tensor-based (DTI) tractography was only able to reconstruct a thin bundle stemming from the left LG and terminating in the PPA (Figure 3).

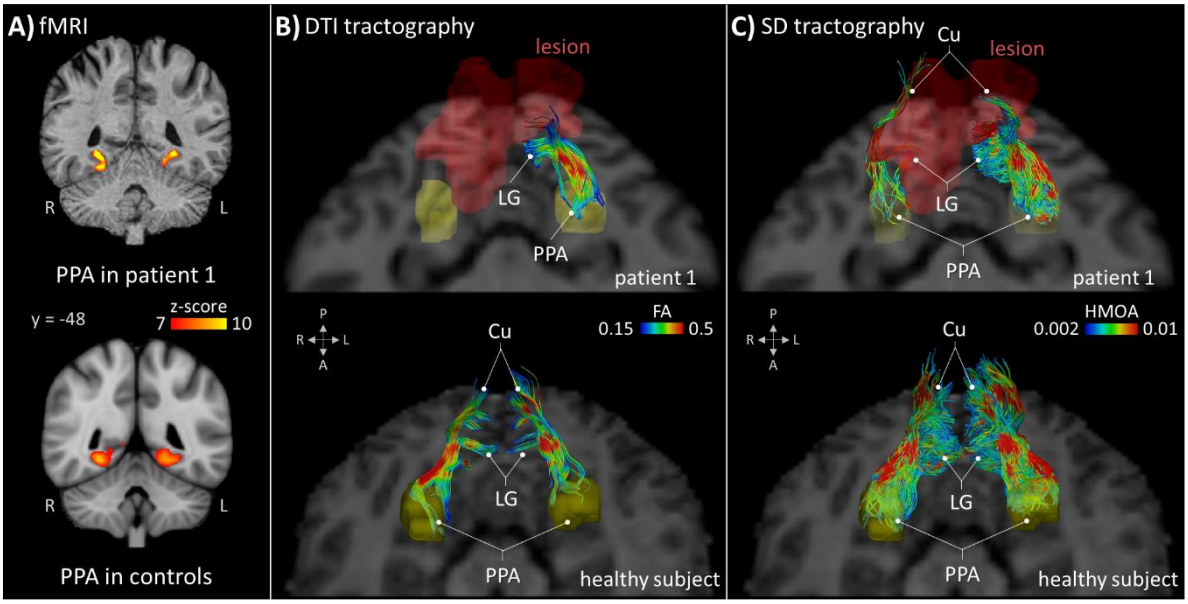

Figure 3. Patient 1 has a responsive PPA with damaged white matter connections to EVC.
(A) The parahippocampal place area (PPA) was identified in Patient 1 as a region of the posterior collateral sulcus that showed stronger responses to images of places compared to those of faces or objects during an fMRI localiser. Mean PPA activations from a control cohort are shown for comparison (Tosoni et al., 2016). **(B)** DTI tractography in Patient 1 was unable to reconstruct connections between early visual cortex (EVC) and the PPA, except for a component stemming from the left LG. An example healthy brain acquired with a similar MRI sequence as the one used for Patient 1 shows that DTI is capable of visualising connections between the PPA and EVC of the Cu and LG. The tract colour overlay corresponds to fractional anisotropy (FA). **(C)** Spherical deconvolution tractography in Patient 1 confirmed the severe damage to connections running between the PPA and EVC. By comparison to the healthy dataset, the component running through the left LG was relatively spared in Patient 1 The tracts are coloured by their hindrance modulated orientational anisotropy (HMOA) (Dell'Acqua et al., 2013), which is a surrogate for fibre density. Cu: cuneus; LG: lingual gyrus.

Data-driven white matter and functional analysis in controls

To explain the findings in Patient 1 given the evidence regarding functional gradients within the PPA, a data-driven clustering analysis was performed to determine whether the PPA's structural connectivity can explain its functional heterogeneity. Structural connectivity was based on 200 diffusion MRI datasets from the Human Connectome Project (HCP) processed with SD tractography, while functional connectivity was based on an average dataset of 812 HCP subjects.

To this end, the whole-brain tractogram of each participant was first converted to a surface-based vertex-wise connectivity matrix. From these matrices, the connections between the PPA on one end, and EVC and an extended RSC region on the other end were selected (Figure 4). These specific connections were selected given the importance of the RSC and many of its neighbouring regions in the spatial learning domain, their close functional involvement with the PPA, and their importance as a relay station between parietal and medial temporal regions according to current visuospatial learning models (Epstein, 2008; Epstein et al., 2007; Kravitz et al., 2011a; Maguire, 2001).

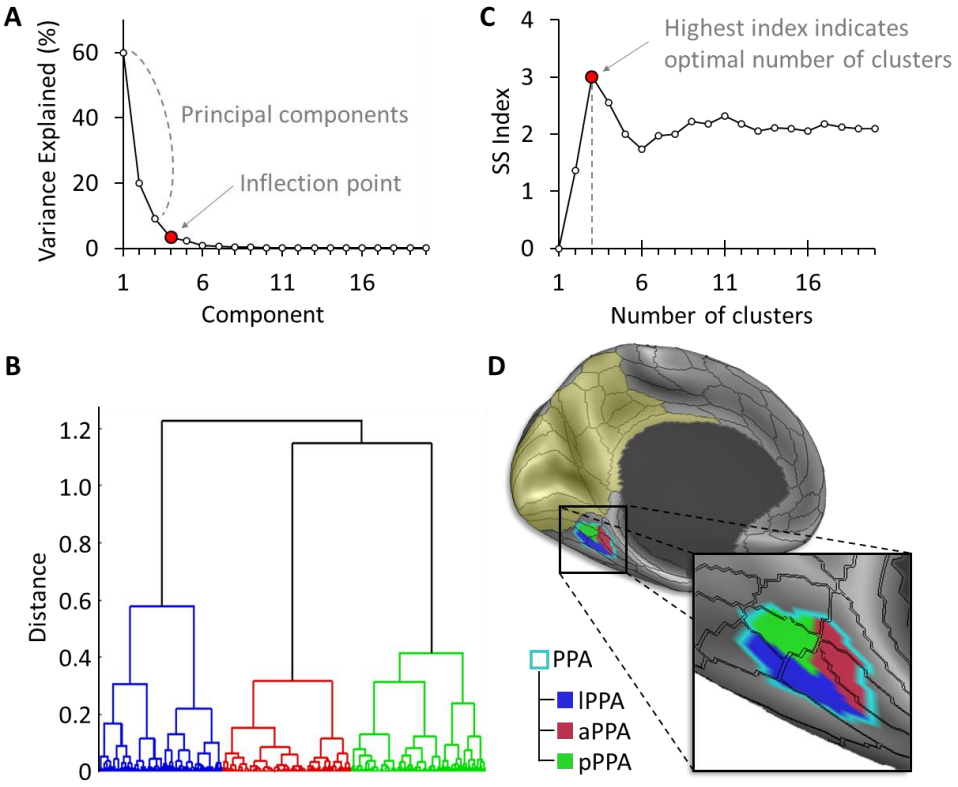

Figure 4. Clustering analysis of the PPA reveals multiple anatomical subunits.
Data-driven clustering of the parahippocampal place area (PPA) based on structural connectivity. **(A)** A principal component analysis (PCA) was used for dimensionality reduction based on the PPA's connectivity to early visual and retrosplenial cortex, and resulted in three principal components. **(B)**, **(C)** Hierarchical agglomerative clustering grouped PPA surface vertices with similar PCA coefficients. The highest separation vs. spread (SS) index (Moreno-Dominguez et al., 2014) was used to objectively determine the optimal number of clusters. **(D)** The resulting anterior, posterior and lateral PPA clusters are shown on the inflated brain surface. Black borders correspond to the MMP atlas (Glasser et al., 2016), and the target region for the structural connectivity is shown in yellow tint.

Principal component analysis (PCA) was used for dimensionality reduction based on the PPA's structural connections to the EVC/RSC region. In both the left and right hemispheres, PCA yielded three principal components which explained 89.1% (LH) and 89.8% (RH) of the variance in the connectivity profile of the PPA to EVC/RSC (Figure 4). The number of components was determined using a 'scree plot' approach (Cattell, 1966) where only the components to the left of the inflection point were retained.

This step was followed by a hierarchical clustering analysis to extract distinct connectivity-based clusters within the PPA. The separation vs. spread (SS) index (Moreno-Dominguez et al., 2014) was used to determine the clustering's optimal granularity (Figure 4). In both hemispheres, a granularity of three clusters yielded the highest SS index: SS_{max} (LH) = 2.71; SS_{max} (RH) = 3.01. This indicated that the PPA is best subdivided into three clusters based on its structural connectivity to the EVC/RSC. Accordingly, three PPA clusters with different structural connectivity profiles emerged: the anterior cluster (aPPA) was mainly connected to the RSC; the posterior cluster (pPPA) was mainly connected to EVC regions V1, V2 and V3; the lateral cluster (lPPA) was partially connected to the ventral portion of EVC region V4 (Figure 5).

To further assess the functional relevance of the resulting clusters, the mean functional connectivity to the EVC/RSC region was also computed for each PPA cluster based on resting-state fMRI dense connectivity maps from the HCP. A pattern emerged that is similar to the one observed with structural connectivity: the aPPA cluster was mainly coupled with RSC, the pPPA cluster with EVC, and the lPPA showed weaker but preferential coupling with EVC (Figure 5).

To confirm the similarity between the structural and functional connectivity results, a Spearman rank correlation analysis indicated that there was indeed a significant agreement between the two for all clusters, in both hemispheres: aPPA (LH): $\rho = .57$, $p < .001$; pPPA (LH): $\rho = .61$, $p < .001$; lPPA (LH): $\rho = .45$, $p < .001$; aPPA (RH): $\rho = .72$, $p < .001$; pPPA (RH): $\rho = .65$, $p < .001$; lPPA (RH): $\rho = .51$, $p < .001$.

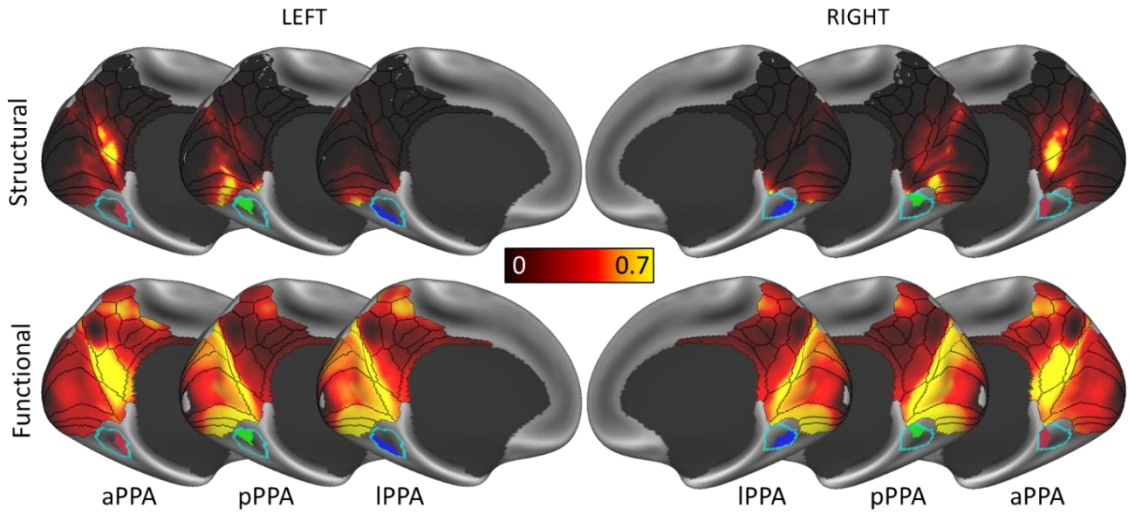

Figure 5. PPA clusters share similar structural and functional connectivity profiles.
Structural (top row) and functional (bottom row) connectivity of the three parahippocampal place area (PPA) clusters. The anterior cluster (aPPA) is preferentially connected to retrosplenial cortex and corresponds to the parieto-medial-temporal branch of the dorsal visual stream (Kravitz et al., 2011a). The posterior cluster (pPPA) is preferentially connected to peripheral representations within early visual cortex (EVC) through the medial occipital longitudinal tract (MOLT). The lateral cluster (lPPA) is more ambiguous but connects more preferentially to EVC. Structural and functional connectivity agree in general, and the main difference between them stems from the spatially smooth and spread nature of functional connectivity. This agreement, especially for the anterior and posterior clusters, lends support to the idea that the PPA is not a single, homogeneous unit and could serve multiple roles within the visuo-spatial processing domain.

White matter bundle connecting EVC and PPA in controls

To isolate the white matter bundles driving the clustering pattern observed in the previous analysis, virtual tractography dissections of 200 HCP subjects were performed. Dissections revealed a large, coherent white matter bundle connecting medial occipital cortex to medial temporal cortex. Within the occipital lobe, this bundle showed the strongest cortical projections in the anterior portions of areas V1, V2 and V3. Within the temporal lobe, the strongest cortical projections fell within the posterior portion of the PPA.

Figure 6 shows the 3D reconstruction of this bundle within the brain surface of an example control participant. After leaving the anterior peri-calcarine cortex with a lateral course, fibres emerging from the Cu and LG merge into a single bundle. This bundle continues anteriorly toward the temporal lobe and terminates in the region that overlaps the anterior tip of the LG and the posterior PHG. The entire course of this bundle is infero-medial to the occipital horn and atrium of the lateral ventricles.

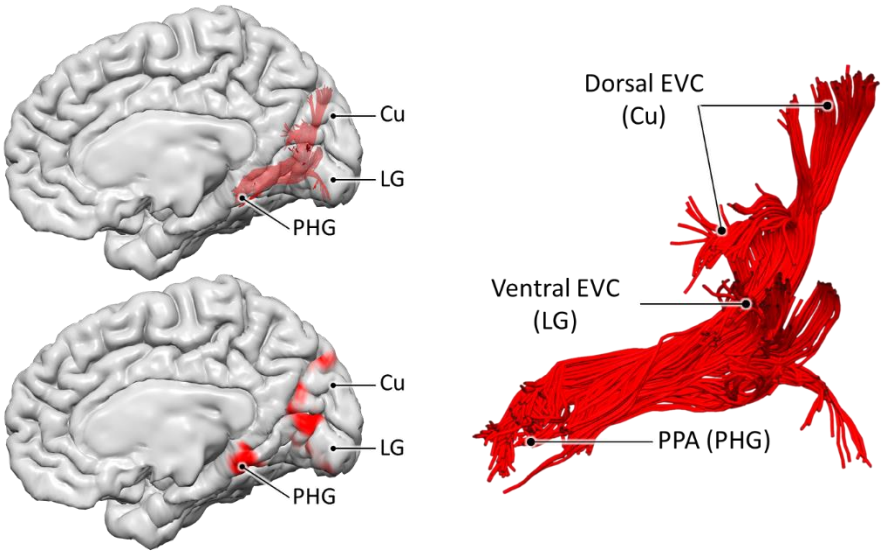

Figure 6. The medial occipital longitudinal tract (MOLT).

The medial occipital longitudinal tract (MOLT) in an example control subject based on spherical deconvolution tractography. The MOLT is an occipito-temporal white matter pathway that stems from the anterior Cu and LG and terminates in the posterior PHG. In the medial occipital lobe, it projects onto peripheral visual field representations within EVC. In the temporal lobe, its terminations overlap the posterior portion of the PPA. Cu: cuneus; LG: lingual gyrus; EVC: early visual cortex; PHG: parahippocampal gyrus; PPA: parahippocampal place area.

Three tractography metrics were then used to compare the spatial distribution of the Cu and LG components of this bundle to each other and across the two hemispheres (Figure 7): the number of streamlines of each component, corrected for length; tract volume (spatial occupancy); and cortical surface area of EVC reached by the tract. Full descriptive statistics for the three metrics are reported in Supplemental Material.

By comparing the two hemispheres, we observed that, for both the Cu and LG components, this bundle is significantly larger, denser and projects to a larger cortical surface area in the right hemisphere. Within each hemisphere, the LG component is significantly larger, denser and projects to a larger cortical surface area than the Cu component. Full statistical analysis results are reported in Supplemental Material and summarised in Figure 7.

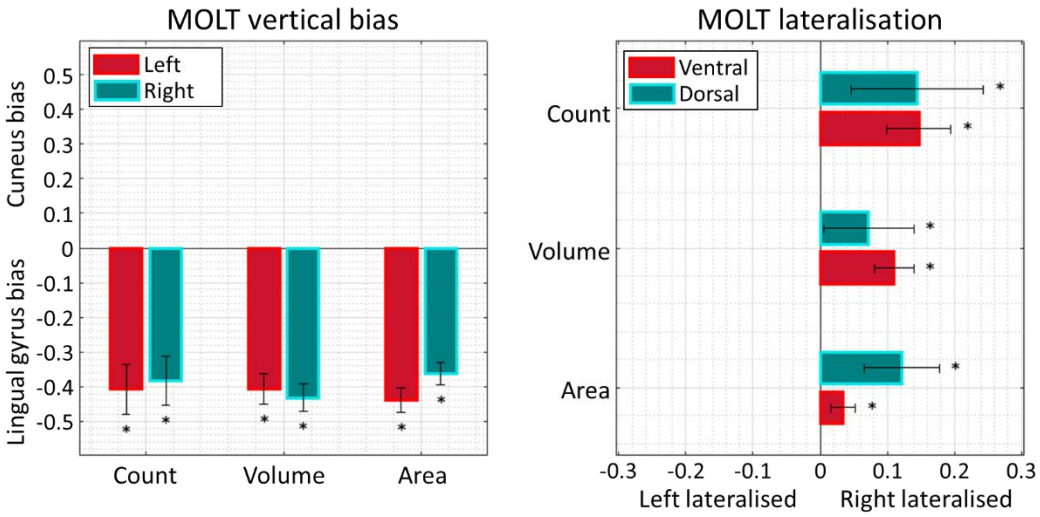

Figure 7. Hemispheric and vertical bias of the MOLT.

The medial occipital longitudinal tract (MOLT) connects the parahippocampal place area (PPA) to peripheral visual field representations within early visual cortex (EVC). The connectivity mediated by the MOLT seems to be stronger in the right hemisphere, and more prominent for the MOLT component that projects to the lingual gyrus. The hemispheric bias is in line with a trend reported in the clinical world where spatial learning deficits are more often associated with right hemisphere lesions. Additionally, the more prominent lingual connections agree with a functional bias toward dorsal visual field representations within the PPA. (*) indicate statistically significant lateralisation and vertical bias based on Bonferroni corrected *p*-values of .0042. 'Count' refers to streamline count corrected for length; 'Volume' refers to the tract's volume (spatial occupancy); 'Area' refers to the cortical surface area reached by the MOLT within EVC. Error bars represent 95% confidence intervals.

DISCUSSION

A new disconnection syndrome of the medial occipital longitudinal tract (MOLT)

Patient 1 presented with acute configuration memory deficits and topographical disorientation following bilateral stroke to the medial occipital lobe. In the chronic stage, neuropsychological assessment revealed that most symptoms receded while deficits in spatial configuration learning persisted. Importantly, Patient 1 had no difficulty recognising familiar faces and objects, nor did he exhibit any impairment in learning new ones. Typically, these observations would be predicted by a focal lesion to the PPA (Bohbot et al., 2015; Malkova and Mishkin, 2003), but structural and functional MRI confirmed that Patient 1's PPA was bilaterally intact and functionally responsive. Therefore, Patient 1 exhibited behavioural deficits typically attributed to focal PPA lesions in the absence of damage to the PPA. According to existing models of visuo-spatial processing, the alternative explanation would be that Patient 1's parietal lobe, classically implicated in spatial processing, would be the origin of his deficit. However, our findings suggest that this may not be the case.

In fact, Patient 1's ability to successfully resume his clay target shooting activity in the chronic stage testifies to effective online integration of residual visuo-spatial information in the classical, parietal dorsal visual stream (Galletti and Fattori, 2018; Goodale and Milner, 1992, 2018). The parietal lobe receives topographically organised information about eye and head orientation, saccadic eye movements and retinal object size directly from the lateral geniculate and pulvinar nuclei of the thalamus (Duhamel et al., 1992; Gamberini et al., 2016; Kaas and Baldwin, 2020; Sincich et al., 2004; Stanton et al., 1977), and indirectly from the superior colliculus (Lyon et al., 2010). These inputs, which are different from the ones that reach EVC, lead to different functional connectivity patterns (Arcaro et al., 2015) and seem to be sufficient for visuomotor integration (Whitwell et al., 2020). In the real world, Patient 1 successfully learned to navigate a novel route and did not show any difficulty in learning and recognising navigationally relevant landmarks. This lends further support to the idea that he can integrate visual, spatial and motor information to perform path integration, and successfully switch between the egocentric and allocentric frames of reference which relies heavily on RSC (although alternative strategies might be employed) (Aguirre and D'Esposito, 1999; Bicanski and Burgess, 2018; Maguire, 2001; van Wijngaarden et al., 2020). This, in addition to the absence of other deficits that would typically arise following parieto-occipital injury (e.g., optic

apraxia), suggests that Patient 1's dorsal visual stream, including the parieto-medial-temporal branch, is fulfilling its role.

However, tractography analysis revealed severe damage to white matter fibres connecting Patient 1's PPA with both lesioned and intact EVC. Such connections are not currently referred to in the literature when discussing visuo-spatial processing, and our data suggest that they play a central role in supporting these functions. This is surprising as evidence for connections between peripheral visual field representations within V2 and the pPHG have been described in the monkey brain using axonal tracing (Gattas, 1997; Schmahmann and Pandya, 2006). There could be several explanations for this oversight. Arguably the ventro-medial regions connected by these fibres are difficult injection targets for axonal tracing studies and they represent a smaller contingent when compared with the foveal projections (Gattas, 1997). Even when these fibres were successfully visualised, they were attributed to other tracts such as the inferior longitudinal fasciculus, or not labelled at all (Schmahmann and Pandya, 2006).

In our analysis of 200 HCP subjects, we consistently replicated a coherent white matter bundle that runs between the peripheral visual representations within EVC (anterior Cu and LG) and the PPA (posterior Cos/PHG and anterior tip of the LG). Considering its medial location and course along the anterior-posterior axis, we refer to this pathway as the medial occipital longitudinal tract (MOLT). The MOLT has a dorsal (Cu) and a ventral (LG) component that both project onto the same zone in the PPA. Fibres of the MOLT were identified in early tractography studies but considered as part of the ventral cingulum (Catani et al., 2002) and inferior longitudinal fasciculus (Catani et al., 2003). The existence of a direct connection between EVC and pPHG as a separate tract from the cingulum was first presented by Catani at the 3rd International School of Clinical Neuroanatomy (2014) and indicated with the descriptive term 'Sledge Runner' fasciculus. Recent *post mortem* dissection and *in vivo* tractography studies confirm the existence of the 'Sledge Runner' fasciculus but they seem to limit its occipital terminations to the dorsal-most portion of the cuneus (Bugain et al., 2021; Koutsarnakis et al., 2019; Vergani et al., 2014). Therefore, we believe that the 'Sledge Runner' fasciculus corresponds to the dorsal-most component of the MOLT, possibly projecting onto dorsal V2 and V3.

Importantly, the MOLT mediates a stronger overall connectivity between the PPA and ventral EVC (LG, upper visual field) compared with dorsal EVC (Cu, lower visual field). This observation is in line with a functional bias within the PPA which contains a substantially larger

representation of the upper visual field (Arcaro et al., 2009; Kravitz et al., 2013; Silson et al., 2015). The MOLT also exhibits a right hemisphere bias, which is an observation that fits existing literature reporting such a hemispheric bias in the spatial learning functions supported by the parietal and medial temporal lobes (Aguirre and D'Esposito, 1999; Maguire, 2001). The two axonal tracing reports we referred to earlier (Gattas, 1997; Schmahmann and Pandya, 2006) used anterograde tracer injections in both EVC and pPHG, which suggests that the MOLT contains reciprocal projections between EVC and the putative site of the macaque PPA.

PPA clusters with different connectivity profiles

The connectivity mediated by the MOLT is a feature that current models of visuo-spatial processing do not capture. The most influential in this category, the revised dual-stream model (Kravitz et al., 2011a, 2013), focuses on input to the MTL via multiple routes. Input that is specific to the PPA seems to arise mainly from indirect parietal projections relayed via the RSC, or from direct projections from V4. This view does not disagree with our findings that different sub-zones within the PPA receive information via separate anatomical pathways. On one hand, we observe that the anterior zone (aPPA) is strongly connected to the RSC, which is a connectivity profile that closely agrees with the descriptions of the parieto-medial-temporal branch of the dual-stream model (Kravitz et al., 2011a) and previous functional connectivity analysis of this pathway (Margulies et al., 2009; Silson et al., 2019). The aPPA cluster also seems to be connected with area prostriata, a small visual area which abuts anterior V1, maps the far periphery and responds to fast motion (Mikellidou et al., 2017). Prostriata might contribute to the aPPA's functions by providing fast motion information important for self-motion stabilisation, especially during changes in head orientation (Tamietto and Leopold, 2018).

On the other hand, the posterior zone (pPPA) is strongly connected to the anterior-most portions of the Cu and LG, overlapping peripheral visual field representations within V2 and V3, and possibly within V1. This observation challenges the current view that EVC projections to the PPA mainly arise from V4, and instead suggests that earlier visual areas contribute directly to PPA afferents. The lateral PPA cluster obtained in our analysis was mainly connected with V4. Although the V4 label used in our study extended dorsally, its connections to the PPA only stemmed from the ventral occipital surface, which is in line with the

descriptions of a ventral V4 (Arcaro et al., 2009; Wang et al., 2015; Winawer et al., 2010; Zeki, 2003).

The idea that the PPA contains multiple subunits with different connectivity profiles has already been alluded to in the literature. Cytoarchitectonic data suggests that Further evidence from task fMRI studies of the human brain suggests that, within the PPA, the posterior portion displays stronger functional coupling with peripheral representations within EVC, while the anterior portion shows a strong coupling with an extended fronto-parietal network (Baldassano et al., 2013, 2016). Additionally, the pPPA contains two distinct retinotopic maps of the visual field, PHC1 and PHC2 (Arcaro et al., 2009), which do not extend to its anterior-most border defined by anatomo-functional approaches (Weiner et al., 2018).

This view of the PPA might seem different from its original description as a cortical region that shows greater functional responses to images of scenes compared to those of isolated faces or objects (Epstein and Kanwisher, 1998). Yet, the two views go together given that the main features in a visual scene are its space-defining elements and the spatial configuration of its constituent elements (Baldassano et al., 2013; Epstein et al., 1999; Kravitz et al., 2011b). Additionally, the PHG plays a general role in processing contextual associations, with spatial associations activating the pPHG and non-spatial associations activating the anterior PHG (Aminoff et al., 2007, 2013; Pihlajamäki et al., 2004).

Our view is that the MOLT carries 'raw' visual information from EVC which the PPA requires, in combination with higher-order spatial information stemming from the parietal lobe, to fully process object configuration. In other words, the MOLT and the parieto-medial-temporal branch of the dual-stream model must work in tandem to allow the PPA to fully carry out its role. The MOLT may carry feedforward and feedback spatial information between EVC and the PPA, thereby serving as a pathway for re-entrant visual information (Hochstein and Ahissar, 2002) that supports a multistage learning of the visual scene and the configuration of objects within it. As such, early activations within the PPA (Bastin et al., 2013a) may correspond to an initial mapping of the 'gist of the scene' which, via feedback to EVC, refines the later, detailed mapping of object configuration. This refined information, still in a retinotopic space, could then be combined with parietal and retrosplenial spatial information at longer latencies (Bastin et al., 2013b), and translated into an allocentric frame of reference. This higher order, viewpoint-invariant spatial information would ultimately reach more anterior MTL regions including the hippocampal formation, and more distant frontal regions

(Dalton and Maguire, 2017; Van Hoesen, 1982; Kravitz et al., 2011a; Schmahmann and Pandya, 2006).

Conclusions

Based on converging evidence from Patient 1 and the HCP cohort, the MOLT may serve as a ventral white matter pathway that carries spatial visual information crucial for configuration learning. In this light, Patient 1 could represent a case of a MOLT disconnection that resulted in a partial deafferentation of the PPA, leading to focal PPA lesion symptoms. Our results shed further light on the notion that the PPA contains multiple functional subunits supported by different anatomical networks.

Limitations and future steps

For this report, we resorted to a multimodal investigation of a clinical case and a large cohort of control participants. It remains important to list some limitations that must be addressed in future investigations. First, although clinical cases offer a rich insight into brain function, they remain problematic and pose a limit on generalisability. Therefore, it is important to extend such investigations to a larger number of cases with similar or even smaller lesions with more selective white matter damage. Second, neuroimaging methods, including fMRI and diffusion, rely on models to produce results. These could therefore vary with data quality or choice of processing pipeline. Finally, future investigations aiming to ascertain the role of the MOLT in the spatial learning domain should include specific testing for its putative function along with imaging investigation within the same control cohort.

ARTICLE DETAILS

Acknowledgements

This work was supported by a Wellcome Trust Investigator Award (No. 103759/Z/14/Z). Data were provided in part by the Human Connectome Project, WU-Minn Consortium (Principal Investigators: David Van Essen and Kamil Ugurbil; 1U54MH091657) funded by the 16 NIH Institutes and Centers that support the NIH Blueprint for Neuroscience Research; and by the McDonnell Center for Systems Neuroscience at Washington University. The authors are grateful to Dr Valentina Sebastiani who performed a general cognitive assessment of Patient 1, and members of the NatBrainLab (www.natbrainlab.co.uk) for their feedback.

Author contributions

Conceptualization, A.B., D.f., and Mar.C.

Methodology, A.B., F.D., C.S., Mas.C., G.Z., D.C., F.D.R., S.D.S., D.f., and Mar.C.

Software, A.B., F.D., D.C., and F.D.R.

Investigation, A.B., C.S., Mas.C., G.Z., Mar.C.

Resources, A.B., F.D., C.S., Mas.C., G.Z., and Mar.C.

Writing – Original Draft, A.B. and Mar.C.

Writing – Review & Editing, A.B., F.D., C.S., Mas.C., G.Z., D.C., F.D.R., S.D.S., D.f., and Mar.C.

Funding Acquisition, C.S., Mas.C., and Mar.C.

METHODS

Configuration learning testing for Patient 1

An adaptation of the task from Bohbot *et al*. (2015) was used to assess implicit learning of configuration and identities. In this task, a standard display containing five cartoon objects in fixed positions on the screen occurs on 80% of trials. On the remaining 20% of trials, one of two possible changes takes place: two of the same objects swap positions but no new objects appear (spatial change, 10% of trials); or one object is replaced by a new one but the four others remain unchanged (identity change, 10% of trials). The task uses multiple object sets, and each set is used for a block of 10 trials during which one object change and one identity change occur at random. To account for Patient 1's visual deficits, each stimulus was presented for 2 s instead of 1.5 s as in the original version of the test, with a 2.5 s interstimulus delay. During the spatial runs, the patient is asked to respond only when a spatial change takes place. During the identity runs, the patient is asked to respond only when an identity change takes place. The score in this test is the fraction of the changes detected by the participant for each the spatial and identity tasks.

The previous test assesses the implicit learning of configuration and identities given that it does not require the patient to name where spatial changes occur, nor does it require them to name the presented objects. Therefore, we developed another test that assesses the ability to explicitly and simultaneously learn the positions of objects in space and their identities. The task starts with a display of a 6x6 square grid with two squares filled with disk tokens which act as placeholders (position does not change throughout the test). Seven additional squares are then filled with items from one of the following categories: portraits of famous persons, cartoons of animals, or letters. The filled matrix is displayed for 5 seconds after which the images and placeholder tokens disappear, and only the empty matrix is displayed. At this stage, the patient is asked to recall the positions and identities of the displayed images. This is repeated until the patient can correctly recall all identities and positions three consecutive times. The score in this test is based on the number of trials required to reach full performance for each of the spatial and identity tasks.

Neuroimaging for Patient 1

Patient 1 gave informed consent in accordance with guidelines set by the Human Studies Committee of G. d'Annunzio University, Chieti. MRI data were acquired from Patient 1 on a 3T Philips Achieva scanner. Structural data were acquired to assess the extent of the ischemic lesion and consisted of the following: a 3D FFE T1-weighted sequence (TR = 8.09 ms; TE = 3.70 ms; flip angle = 8°; voxel size = 1x1x1 mm^3; 160 slices); axial T2-weighted (TR = 3 s; TE = 80 ms; flip angle = 90°; voxel size = 0.5x0.5x3.6 mm^3; 39 slices); and FLAIR (TR = 11 s; TE = 125 ms; flip angle = 90°; voxel size = 0.5x0.5x4 mm^3; 30 slices) sequences.

The PPA in Patient 1 was identified using a 'places vs. faces' functional MRI task. The same task was previously used by Tosoni et al. (2016) in a set of control participants (N = 39). Briefly, it consisted of displays showing images of places and images of faces (shades of gray, 240×240 pixels) in alternating blocks (16 s) while Patient 1 fixated on the centre of the display. Each image presentation lasted for 300 ms followed by a 200 ms delay (fixation only). Blocks were separated by fixation-only rest periods of variable durations (mean = 13 s). Two runs were collected, each including 16 blocks of images of faces and places. Functional data were acquired using a gradient-echo EPI sequence with the following parameters: TR = 1.91s; TE = 25 ms; flip angle = 80°; 39 contiguous oblique axial slices acquired in ascending interleaved order; voxel size = 3.59×3.59×3.59 mm^3). Pre-processing and data analysis were performed using in-house software (fIDL) developed at Washington University in St. Louis. Briefly, pre-processing included motion-correction within and between runs, slice timing correction, intensity normalisation between runs, resampling into 3 mm^3 isotropic voxels, and spatial normalisation into the standardised 711–2C atlas space (Van Essen, 2005; Talairach and Tournoux, 1988). Functional images were analysed using a general linear model (GLM). Responses to place and face blocks were generated by convolving a function representing the duration of the process (rectangle function) with a standard hemodynamic response function (Boynton et al., 1996). Place-selective regions were defined from the contrast between place vs. face activation maps. More details about data analysis can be found in Tosoni et al. (2016).

Diffusion-weighted MRI (DWI) was acquired using a spin-echo echo planar imaging sequence (TE = 102.98 ms; TR = 8.51 s; 60 slices; slice thickness = 2 mm; matrix size = 112x112; voxel size = 2x2 mm^2; 60 gradient directions; b = 1500 s/mm^2; one non-diffusion-weighted volume). DWI data were first corrected for noise (Veraart et al., 2016) and Gibbs ringing artefacts (Kellner et al., 2016). Motion and eddy-current distortions were corrected using *eddy*

(Andersson and Sotiropoulos, 2016) with outlier slice replacement (Andersson et al., 2016). To correct for EPI susceptibility distortions, the anisotropic power map (Dell'Acqua et al., 2014) was 'unwarped' to the T1w image using the symmetric normalisation algorithm in ANTs (Avants et al., 2008, 2011) confined to the phase encoding axis. The resulting transformations were applied to the *eddy* output, effectively resulting in DWI images that are in register with the structural data.

Tractography was computed using StarTrack (https://www.mr-startrack.com/). Tractography based on the tensor model (DTI) was performed using an Euler algorithm and the following parameters: minimum FA threshold = 0.15; maximum angle = 35°; step size = 1 mm; minimum streamline length = 20 mm; maximum streamline length = 300 mm. Spherical deconvolution was based on a damped version of the Richardson-Lucy algorithm (Dell'Acqua et al., 2010, 2013) with the following parameters: fibre response α = 1.5; number of iterations = 300; amplitude threshold η = 0.0015; geometric regularisation ν = 16. Fibre tracking was performed using the dispersion tracking algorithm using the following parameters: minimum HMOA threshold = 0.003; maximum dispersion angle = 30°; bootstrapping runs = 10; minimum streamline length = 20 mm; maximum streamline length = 300 mm. Virtual dissections were performed in TrackVis (http://trackvis.org).

Neuroimaging for controls

DWI data from 200 healthy participants (100 females; age = 29.16 ± 3.73 years) were obtained from the Human Connectome Project (https://www.humanconnectome.org). All subjects were right-handed as determined by a score of 50 and above on the Edinburgh handedness questionnaire (Oldfield, 1971).

Diffusion MRI data of the HCP were acquired on a 3 T Siemens "Connectome Skyra" using a spin-echo EPI sequence (TR = 5520 ms; TE = 89.5 ms; matrix of 168x144; 111 slices with a thickness of 1.25 mm; isotropic voxels of 1.25 mm; multiband factor = 3). Three diffusion-weighted shells were acquired (b = 1000, 2000 and 3000 s/mm^2) with two opposite phase-encoding directions each (L>>R and R>>L). Each shell consisted of 90 diffusion-weighted directions and six interleaved non-diffusion-weighted volumes. For this study, only data from the b = 2000 s/mm^2 shell were used as this b-value offers a good compromise between signal-

to-noise ratio and high angular resolution, especially at high spatial resolution (Dell'Acqua and Tournier, 2019).

The data were obtained from the HCP database in pre-processed form following the HCP minimal pre-processing pipelines (Glasser et al., 2013). Briefly, correction for motion and eddy current distortions was performed using *eddy* with outlier slice replacement (Andersson and Sotiropoulos, 2016; Andersson et al., 2016). Correction of susceptibility distortions was incorporated into this step by means of an off-resonance field estimated using *topup* (Andersson et al., 2003). Diffusion MRI data were then corrected for gradient non-linearity and finally aligned to the structural space using a boundary-based registration (Greve and Fischl, 2009).

Tractography was computed using StarTrack (https://www.mr-startrack.com/). Spherical deconvolution was based on a damped version of the Richardson-Lucy algorithm (Dell'Acqua et al., 2010, 2013) with the following parameters: fibre response α = 1.8; number of iterations = 300; amplitude threshold η = 0.0020; geometric regularisation ν = 12. Fibre tracking was then performed using the Euler-like algorithm and the following parameters: minimum HMOA threshold = 0.0033; step size = 1.0 mm; maximum angle threshold = 45°; minimum fibre length = 20 mm; maximum fibre length = 300 mm.

Building vertex-wise connectivity matrices

The whole-brain tractogram of each subject was converted to a vertex-wise structural connectivity matrix. For each subject, this approach was based on the native space midthickness cortical mesh, vertex-matched to the '32k FS LR' surface template using the multimodal surface matching (MSM) method (Glasser et al., 2016; Robinson et al., 2014). These surfaces have the advantage of maintaining the native anatomy of the brain while offering a vertex-level matching between subjects. As a result, information from multiple subjects can be directly compared at each vertex.

The end points of each tractography streamline were projected to the nearest vertex on the midthickness surface, with a maximum allowed distance of 4 mm. Only streamlines that resulted in two cortical targets (one for each end point) survived this step. Due to the sparse distribution of streamlines near the cortical surface, this approach would result in a patchy

representation of cortical targets which is problematic for group-level analysis. To compensate for this and for tractography's uncertainty near grey matter (Jones, 2003), a geodesic Gaussian kernel (FWHM = 2.5 mm) was applied to each target independently. The connectivity information resulting from each streamline was used to populate a 32492 x 32492 sparse matrix representing all vertices of the cortical surface. Each subject's matrix was then normalised by its highest value before the group-level mean connectivity matrix was computed.

Defining cortical ROIs

In preparation for the PPA clustering analysis (next section), two cortical regions of interest (ROIs) were defined using published cortical atlases. First, a ROI covering the PPA was obtained from Weiner et al. (2018) who demonstrated that the location of functional responses within the PPA can be predicted with high accuracy using surface topology alone. The ROI covered parts of the posterior CoS and PHG, and anterior LG. This ROI overlaps the following labels from the multimodal parcellation (MMP) atlas (Glasser et al., 2016): VMV1, VMV2, VMV3, PHA1, PHA2 and PHA3. The ROI was released by the authors in the form of a FreeSurfer label registered to the 'fsaverage' template, which we subsequently realigned to the '32k_FS_LR' template following HCP guidelines.

The second ROI included the following labels from the MMP atlas (Glasser et al., 2016): V1, V2, V3, V4, V3A, V6, ProS, DVT, POS1, POS2, 7m, 7Pm, 7Am, PCV, 31pd, 31pv, 31a, d23ab, v23ab and RSC. This effectively covered the cuneus (Cu), lingual gyrus (LG) and occipital pole (OP) and included all eccentricity representations within EVC. Additionally, it covered cortical areas that relay information from the parietal lobe to the MTL according to the dual-stream model (Kravitz et al., 2011a) and are important for spatial learning based on human case studies (Maguire, 2001). It also included other neighbouring labels of the MMP atlas to ensure the ROI's spatial continuity.

PPA clustering and connectivity analysis

The aim of this analysis was to assess whether the PPA contains multiple sub-units with different anatomical connectivity profiles based on a data-driven approach. First, the values of the subject-level connectivity matrices previously computed were converted to z-scores

(Thiebaut de Schotten et al., 2014), and the mean z-matrix was computed. This matrix was then filtered to only retain the connections between the PPA on one end, and both the EVC and RSC ROIs on the other end.

The mean z-matrix was entered into a principal component analysis (PCA). In this context, the z-matrix acted as a large dataset where the PPA vertices represented variables and the EVC/RSC vertices represented observations of these variables. This approach was blind to the locations of vertices on the brain surface and was thus completely driven by the connectivity profile of each PPA vertex. A scree plot (Cattell, 1966) was used to determine the number of components to retain. The resulting principal components effectively represented the PPA region in a reduced space of only a few variables. Importantly, this step also acted as a filter that suppressed contributions from 'noisy' connections, or ones which had very high inter-subject variability.

Agglomerative hierarchical clustering (Euclidean distance, ward algorithm) was applied to the resulting principal component coefficients to extract binary clusters within the PPA. This approach resulted in a dendrogram (hierarchy tree) where each observation (PPA vertex) was linked to other observations in a hierarchical fashion. These links defined clusters of vertices that were most similar in their loadings on the principal components. The spread vs. separation (SS) index proposed by Moreno-Dominguez et al. (2014) was used to objectively determine the optimal number of clusters. A higher SS index means that the variability of observations between clusters is greater than the variability within clusters. Therefore, the number of clusters was chosen to correspond to the highest SS index.

The mean structural connectivity of each resulting cluster was then obtained from the mean connectivity matrix previously computed. Additionally, the mean functional connectivity of each cluster was calculated based on the group average dense resting-state functional connectome released by the HCP as part of the 'HCP-S1200_GroupAvg_v1' dataset. Tract-based connectivity values, which follow a heavily skewed distribution compared to functional connectivity, were log-transformed (Donahue et al., 2016; Moreno-Dominguez et al., 2014). Spearman rank correlations (one-tailed) were then computed between tract-based and functional connectivity measures for each cluster to assess the degree of agreement between the two modalities.

Virtual dissections

Virtual dissections were performed in TrackVis (http://trackvis.org/) to isolate the anatomical bundle that gave rise to the observed connectivity patterns between the posterior PPA cluster and the EVC in the clustering analysis.

MegaTrack (Dell'Acqua et al., 2015), a supervised semi-automatic group-level approach, was used to handle the large number of participants. Each participant's anisotropic power map (Dell'Acqua et al., 2014) was mapped to the space of the MNI152 template using the symmetric normalisation algorithm in ANTs (Avants et al., 2008, 2011). The resulting affine and diffeomorphic warping were applied to each participant's tractogram and all tractograms were concatenated to create a single 'mega' tractography dataset. After performing virtual dissections of the large dataset in common space, each participant's streamlines were mapped back to native space where tract-specific measurements could be extracted, and cortical projections analysed.

To isolate the tracts of interest, a ROI was manually defined on sagittal and coronal slices to intersect any streamlines entering the medial occipital lobe, covering the LG and Cu. A sphere ROI was defined at the intersection between the LG and PHG, overlapping the anatomical location of the PPA. Only streamlines terminating within the PPA ROI and crossing the occipital ROI were retained. Additional ROIs were used to manually refine the dissected tracts and remove spurious streamlines (e.g., streamlines that took unusually long trajectories or crossed sulcal boundaries).

Assessment of lateralisation and vertical bias in the dissected tracts

Hemispheric lateralisation for each of the dorsal and ventral components was assessed according to the following formula:

$$lateralisation = \frac{value_{right} - value_{left}}{value_{right} + value_{left}}$$

where *value* represents one of the following metrics: (1) streamline count, corrected for distance; (2) tract volume; (3) surface area of connected EVC cortex. In this way, a right hemisphere bias would lead to positive values.

Additionally, given that that PPA contains a substantially larger representation of the upper visual field (Arcaro et al., 2009; Silson et al., 2015), the connectivity between the PPA and ventral EVC (representing the upper visual field) was expected to be stronger than that with dorsal EVC (representing the lower visual field). This vertical bias was assessed following a similar approach to the one used for lateralisation, according to the following formula:

$$vertical\ bias = \frac{value_{dorsal} - value_{ventral}}{value_{dorsal} + value_{ventral}}$$

where *value* also represents one the previously described metrics, and where a ventral bias would result in negative values.

For each of these comparisons, statistical significance was determined through a one sample t-test (two-tailed) performed on the resulting bias index. The Bonferroni corrected significance level was set to 0.0042.

REFERENCES

Aguirre, G.K., and D'Esposito, M. (1999). Topographical disorientation: A synthesis and taxonomy. Brain *122*, 1613–1628.

Aguirre, G.K., Detre, J.A., Alsop, D.C., and D'Esposito, M. (1996). The parahippocampus subserves topographical learning in man. Cereb. Cortex *6*, 823–829.

Aminoff, E., Gronau, N., and Bar, M. (2007). The parahippocampal cortex mediates spatial and nonspatial associations. Cereb. Cortex *17*, 1493–1503.

Aminoff, E.M., Kveraga, K., and Bar, M. (2013). The role of the parahippocampal cortex in cognition. Trends Cogn. Sci. *17*, 379–390.

Andersson, J.L.R., and Sotiropoulos, S.N. (2016). An integrated approach to correction for off-resonance effects and subject movement in diffusion MR imaging. Neuroimage *125*, 1063–1078.

Andersson, J.L.R., Skare, S., and Ashburner, J. (2003). How to correct susceptibility distortions in spin-echo echo-planar images: Application to diffusion tensor imaging. Neuroimage *20*, 870–888.

Andersson, J.L.R., Graham, M.S., Zsoldos, E., and Sotiropoulos, S.N. (2016). Incorporating outlier detection and replacement into a non-parametric framework for movement and distortion correction of diffusion MR images. Neuroimage *141*, 556–572.

Arcaro, M.J., McMains, S.A., Singer, B.D., and Kastner, S. (2009). Retinotopic organization of human ventral visual cortex. J. Neurosci. *29*, 10638–10652.

Arcaro, M.J., Pinsk, M.A., and Kastner, S. (2015). The anatomical and functional organization of the human visual pulvinar. J. Neurosci. *35*, 9848–9871.

Avants, B.B., Epstein, C.L., Grossman, M., and Gee, J.C. (2008). Symmetric diffeomorphic image registration with cross-correlation: Evaluating automated labeling of elderly and neurodegenerative brain. Med. Image Anal. *12*, 26–41.

Avants, B.B., Tustison, N.J., Song, G., Cook, P.A., Klein, A., and Gee, J.C. (2011). A reproducible evaluation of ANTs similarity metric performance in brain image registration. Neuroimage *54*, 2033–2044.

Baldassano, C., Beck, D.M., and Fei-Fei, L. (2013). Differential connectivity within the Parahippocampal Place Area. Neuroimage *75*, 236–245.

Baldassano, C., Fei-Fei, L., and Beck, D.M. (2016). Pinpointing the peripheral bias in neural scene-processing networks during natural viewing. J. Vis. *16*, 1–14.

Bastin, J., Vidal, J.R., Bouvier, S., Perrone-Bertolotti, M., Benis, D., Kahane, P., David, O., Lachaux, J.-P., and Epstein, R.A. (2013a). Temporal components in the parahippocampal place area revealed by human intracerebral recordings. J. Neurosci. *33*, 10123–10131.

Bastin, J., Committeri, G., Kahane, P., Galati, G., Minotti, L., Lachaux, J.P., and Berthoz, A. (2013b). Timing of posterior parahippocampal gyrus activity reveals multiple scene processing stages. Hum. Brain Mapp. *34*, 1357–1370.

Bicanski, A., and Burgess, N. (2018). A neural-level model of spatial memory and imagery. Elife *7*, e33752.

Boccia, M., Sulpizio, V., Nemmi, F., Guariglia, C., and Galati, G. (2017). Direct and indirect parieto-medial temporal pathways for spatial navigation in humans: evidence from resting-state functional connectivity. Brain Struct. Funct. *222*, 1945–1957.

Bohbot, V.D., Kalina, M., Stepankova, K., Spackova, N., Petrides, M., and Nadel, L. (1998). Spatial

memory deficits in patients with lesions to the right hippocampus and to the right parahippocampal cortex. Neuropsychologia *36*, 1217–1238.

Bohbot, V.D., Allen, J.J.B., Dagher, A., Dumoulin, S.O., Evans, A.C., Petrides, M., Kalina, M., Stepankova, K., and Nadel, L. (2015). Role of the parahippocampal cortex in memory for the configuration but not the identity of objects: converging evidence from patients with selective thermal lesions and fMRI. Front. Hum. Neurosci. *9*, 431.

Boynton, G.M., Engel, S.A., Glover, G.H., and Heeger, D.J. (1996). Linear systems analysis of functional magnetic resonance imaging in human V1. J. Neurosci. *16*, 4207–4221.

Bugain, M., Dimech, Y., Torzhenskaya, N., Thiebaut de Schotten, M., Caspers, S., Muscat, R., and Bajada, C.J. (2021). Occipital Intralobar fasciculi: a description, through tractography, of three forgotten tracts. Commun. Biol. *4*, 433.

Burgess, N., Maguire, E.A., and O'Keefe, J. (2002). The human hippocampus and spatial and episodic memory. Neuron *35*, 625–641.

Catani, M., Howard, R.J., Pajevic, S., and Jones, D.K. (2002). Virtual in vivo interactive dissection of white matter fasciculi in the human brain. Neuroimage *17*, 77–94.

Catani, M., Jones, D.K., Donato, R., and Ffytche, D.H. (2003). Occipito-temporal connections in the human brain. Brain *126*, 2093–2107.

Cattell, R.B. (1966). The scree test for the number of factors. Multivariate Behav. Res. *1*, 245–276.

Dalton, M.A., and Maguire, E.A. (2017). The pre/parasubiculum: A hippocampal hub for scene-based cognition? Curr. Opin. Behav. Sci. *17*, 34–40.

Dell'Acqua, F., and Tournier, J. -Donal. (2019). Modelling white matter with spherical deconvolution: How and why? NMR Biomed. *32*, e3945.

Dell'Acqua, F., Scifo, P., Rizzo, G., Catani, M., Simmons, A., Scotti, G., and Fazio, F. (2010). A modified damped Richardson-Lucy algorithm to reduce isotropic background effects in spherical deconvolution. Neuroimage *49*, 1446–1458.

Dell'Acqua, F., Simmons, A., Williams, S.C.R., and Catani, M. (2013). Can spherical deconvolution provide more information than fiber orientations? Hindrance modulated orientational anisotropy, a true-tract specific index to characterize white matter diffusion. Hum. Brain Mapp. *34*, 2464–2483.

Dell'Acqua, F., Lacerda, L., Catani, M., and Simmons, A. (2014). Anisotropic Power maps: A diffusion contrast to reveal low anisotropy tissues from HARDI data. In Proceedings Joint Annual Meeting ISMRM/ESMRMB, (Milan), p. 0730.

Dell'Acqua, F., Lacerda, L., Barrett, R., D'Anna, L., Tsermentseli, S., Goldstein, L., and Catani, M. (2015). MegaTrack : A fast and effective strategy for group comparison and supervised analysis of large-scale tractography datasets. Proc. Int. Soc. Magn. Reson. Med. *23*, 2843.

Donahue, C.J., Sotiropoulos, S.N., Jbabdi, S., Hernandez-Fernandez, M., Behrens, T.E., Dyrby, T.B., Coalson, T., Kennedy, H., Knoblauch, K., Van Essen, D.C., et al. (2016). Using diffusion tractography to predict cortical connection strength and distance: A quantitative comparison with tracers in the monkey. J. Neurosci. *36*, 6758–6770.

Duhamel, J.R., Colby, C.L., and Goldberg, M.E. (1992). The updating of the representation of visual space in parietal cortex by intended eye movements. Science (80-.). *255*, 90–92.

Epstein, R.A. (2008). Parahippocampal and retrosplenial contributions to human spatial navigation. Trends Cogn. Sci. *12*, 388–396.

Epstein, R., and Kanwisher, N. (1998). A cortical representation of the local visual environment. Nature *392*, 598–601.

Epstein, R., Harris, A., Stanley, D., and Kanwisher, N. (1999). The parahippocampal place area: Recognition, navigation, or encoding? Neuron *23*, 115–125.

Epstein, R.A., Parker, W.E., and Feiler, A.M. (2007). Where am I now? Distinct roles for parahippocampal and retrosplenial cortices in place recognition. J. Neurosci. *27*, 6141–6149.

Van Essen, D.C. (2005). A Population-Average, Landmark- and Surface-based (PALS) atlas of human cerebral cortex. Neuroimage *28*, 635–662.

Galletti, C., and Fattori, P. (2018). The dorsal visual stream revisited: Stable circuits or dynamic pathways? Cortex *98*, 203–217.

Gamberini, M., Bakola, S., Passarelli, L., Burman, K.J., Rosa, M.G.P., Fattori, P., and Galletti, C. (2016). Thalamic projections to visual and visuomotor areas (V6 and V6A) in the rostral bank of the parieto-occipital sulcus of the Macaque. Brain Struct. Funct. *221*, 1573–1589.

Gattas, R. (1997). Cortical projections of area V2 in the macaque. Cereb. Cortex *7*, 110–129.

Glasser, M.F., Sotiropoulos, S.N., Wilson, J.A., Coalson, T.S., Fischl, B., Andersson, J.L., Xu, J., Jbabdi, S., Webster, M., Polimeni, J.R., et al. (2013). The minimal preprocessing pipelines for the Human Connectome Project. Neuroimage *80*, 105–124.

Glasser, M.F., Coalson, T.S., Robinson, E.C., Hacker, C.D., Harwell, J., Yacoub, E., Ugurbil, K., Andersson, J., Beckmann, C.F., Jenkinson, M., et al. (2016). A multi-modal parcellation of human cerebral cortex. Nature *536*, 171–178.

Goodale, M.A., and Milner, A.D. (1992). Separate visual pathways for perception and action. Trends Neurosci. *15*, 20–25.

Goodale, M.A., and Milner, A.D. (2018). Two visual pathways – Where have they taken us and where will they lead in future? Cortex *98*, 283–292.

Greve, D.N., and Fischl, B. (2009). Accurate and robust brain image alignment using boundary-based registration. Neuroimage *48*, 63–72.

Hochstein, S., and Ahissar, M. (2002). View from the top: Hierarchies and reverse hierarchies in the visual system. Neuron *36*, 791–804.

Van Hoesen, G.W. (1982). The parahippocampal gyrus: New observations regarding its cortical connections in the monkey. Trends Neurosci. *5*, 345–350.

Jones, D.K. (2003). Determining and visualizing uncertainty in estimates of fiber orientation from diffusion tensor MRI. Magn. Reson. Med. *49*, 7–12.

Kaas, J.H., and Baldwin, M.K.L. (2020). The evolution of the pulvinar complex in primates and its role in the dorsal and ventral streams of cortical processing. Vision *4*, 3.

Kellner, E., Dhital, B., Kiselev, V.G., and Reisert, M. (2016). Gibbs-ringing artifact removal based on local subvoxel-shifts. Magn. Reson. Med. *76*, 1574–1581.

Konen, C.S., Behrmann, M., Nishimura, M., and Kastner, S. (2011). The functional neuroanatomy of object agnosia: A case study. Neuron *71*, 49–60.

Koutsarnakis, C., Kalyvas, A. V., Skandalakis, G.P., Karavasilis, E., Christidi, F., Komaitis, S., Velonakis, G., Liakos, F., Emelifeonwu, J., Giavri, Z., et al. (2019). Sledge runner fasciculus: Anatomic architecture and tractographic morphology. Brain Struct. Funct. *224*, 1051–1066.

Kravitz, D.J., Saleem, K.S., Baker, C.I., and Mishkin, M. (2011a). A new neural framework for visuospatial processing. Nat. Rev. Neurosci. *12*, 217–230.

Kravitz, D.J., Peng, C.S., and Baker, C.I. (2011b). Real-world scene representations in high-level visual cortex: It's the spaces more than the places. J. Neurosci. *31*, 7322–7333.

Kravitz, D.J., Saleem, K.S., Baker, C.I., Ungerleider, L.G., and Mishkin, M. (2013). The ventral visual pathway: An expanded neural framework for the processing of object quality. Trends Cogn. Sci. *17*, 26–49.

Lyon, D.C., Nassi, J.J., and Callaway, E.M. (2010). A disynaptic relay from superior colliculus to dorsal stream visual cortex in Macaque Monkey. Neuron *65*, 270–279.

Maguire, E. (2001). The retrosplenial contribution to human navigation: A review of lesion and neuroimaging findings. Scand. J. Psychol. *42*, 225–238.

Maguire, E.A., Frith, C.D., Burgess, N., Donnett, J.G., and O'Keefe, J. (1998). Knowing where things are: Parahippocampal involvement in encoding object locations in virtual large-scale space. J. Cogn. Neurosci. *10*, 61–76.

Maguire, E.A., Gadian, D.G., Johnsrude, I.S., Good, C.D., Ashburner, J., Frackowiak, R.S., and Frith, C.D. (2000). Navigation-related structural change in the hippocampi of taxi drivers. Proc. Natl. Acad. Sci. *97*, 4398–4403.

Malkova, L., and Mishkin, M. (2003). One-trial memory for object-place associations after separate lesions of hippocampus and posterior parahippocampal region in the monkey. J. Neurosci. *23*, 1956–1965.

Margulies, D.S., Vincent, J.L., Kelly, C., Lohmann, G., Uddin, L.Q., Biswal, B.B., Villringer, A., Castellanos, F.X., Milham, M.P., and Petrides, M. (2009). Precuneus shares intrinsic functional architecture in humans and monkeys. Proc. Natl. Acad. Sci. *106*, 20069–20074.

Mcnaughton, B.L., Leonard, B., and Chen, L. (1989). Cortical-hippocampal interactions and cognitive mapping: A hypothesis based on reintegration of the parietal and inferotemporal pathways for visual processing. Psychobiology *17*, 230–235.

Mikellidou, K., Kurzawski, J.W., Frijia, F., Montanaro, D., Greco, V., Burr, D.C., and Morrone, M.C. (2017). Area prostriata in the human brain. Curr. Biol. *27*, 3056-3060.e3.

Mishkin, M., Ungerleider, L.G., and Macko, K. (1983). Object vision and spatial vision: two cortical pathways. Trends Neurosci. *6*, 414–417.

Moreno-Dominguez, D., Anwander, A., and Knösche, T.R. (2014). A hierarchical method for whole-brain connectivity-based parcellation. Hum. Brain Mapp. *35*, 5000–5025.

O'Keefe, J., and Dostrovsky, J. (1971). The hippocampus as a spatial map: Preliminary evidence from unit activity in the freely-moving rat. Brain Res. *34*, 171–175.

Oldfield, R.C. (1971). The assessment and analysis of handedness: The Edinburgh Inventory. Neuropsychologia *9*, 97–113.

Owen, A.M., Milner, B., Petrides, M., and Evans, A.C. (1996). A specific role for the right parahippocampal gyrus in the retrieval of object-location: A positron emission tomography study. J. Cogn. Neurosci. *8*, 588–602.

Pihlajamäki, M., Tanila, H., Könönen, M., Hänninen, T., Hämäläinen, A., Soininen, H., and Aronen, H.J. (2004). Visual presentation of novel objects and new spatial arrangements of objects differentially activates the medial temporal lobe subareas in humans. Eur. J. Neurosci. *19*, 1939–1949.

Ploner, C.J., Gaymard, B.M., Rivaud-Péchoux, S., Baulac, M., Clémenceau, S., Samson, S., and Pierrot-Deseilligny, C. (2000). Lesions affecting the parahippocampal cortex yield spatial memory deficits in humans. Cereb. Cortex *10*, 1211–1216.

Robinson, E.C., Jbabdi, S., Glasser, M.F., Andersson, J., Burgess, G.C., Harms, M.P., Smith, S.M., Van Essen, D.C., and Jenkinson, M. (2014). MSM: A new flexible framework for Multimodal Surface Matching. Neuroimage *100*, 414–426.

Schmahmann, J.D., and Pandya, D.N. (2006). Fiber pathways of the brain (Oxford: Oxford University Press).

Silson, E.H., Chan, A.W.-Y., Reynolds, R.C., Kravitz, D.J., and Baker, C.I. (2015). A retinotopic basis for the division of high-level scene processing between lateral and ventral human occipitotemporal cortex. J. Neurosci. *35*, 11921–11935.

Silson, E.H., Steel, A., Kidder, A., Gilmore, A.W., and Baker, C.I. (2019). Distinct subdivisions of human medial parietal cortex support recollection of people and places. Elife *8*, e47391.

Sincich, L.C., Park, K.F., Wohlgemuth, M.J., and Horton, J.C. (2004). Bypassing V1: A direct geniculate input to area MT. Nat. Neurosci. *7*, 1123–1128.

Stanton, G.B., Cruce, W.L.R., Goldberg, M.E., and Robinson, D.L. (1977). Some ipsilateral projections to areas PF and PG of the inferior parietal lobule in monkeys. Neurosci. Lett. *6*, 243–250.

Talairach, J., and Tournoux, P. (1988). Co-planar stereotaxic atlas of the human brain: 3-dimensional proportional system : An approach to cerebral imaging (Stuttgart: Georg Thieme).

Tamietto, M., and Leopold, D.A. (2018). Visual cortex: The eccentric area prostriata in the human brain. Curr. Biol. *28*, R17–R19.

Thiebaut de Schotten, M., Urbanski, M., Valabregue, R., Bayle, D.J., and Volle, E. (2014). Subdivision of the occipital lobes: An anatomical and functional MRI connectivity study. Cortex *56*, 121–137.

Tosoni, A., Guidotti, R., Del Gratta, C., Committeri, G., and Sestieri, C. (2016). Preferential coding of eye/hand motor actions in the human ventral occipito-temporal cortex. Neuropsychologia *93*, 116–127.

Veraart, J., Fieremans, E., and Novikov, D.S. (2016). Diffusion MRI noise mapping using random matrix theory. Magn. Reson. Med. *76*, 1582–1593.

Vergani, F., Mahmood, S., Morris, C.M., Mitchell, P., and Forkel, S.J. (2014). Intralobar fibres of the occipital lobe: A post mortem dissection study. Cortex *56*, 145–156.

Wang, L., Mruczek, R.E.B., Arcaro, M.J., and Kastner, S. (2015). Probabilistic maps of visual topography in human cortex. Cereb. Cortex *25*, 3911–3931.

Weiner, K.S., Barnett, M.A., Witthoft, N., Golarai, G., Stigliani, A., Kay, K.N., Gomez, J., Natu, V.S., Amunts, K., Zilles, K., et al. (2018). Defining the most probable location of the parahippocampal place area using cortex-based alignment and cross-validation. Neuroimage *170*, 373–384.

Whitwell, R.L., Sperandio, I., Buckingham, G., Chouinard, P.A., and Goodale, M.A. (2020). Grip constancy but not perceptual size constancy survives lesions of early visual cortex. Curr. Biol. *30*, 3680-3686.e5.

van Wijngaarden, J.B.G., Babl, S.S., and Ito, H.T. (2020). Entorhinal-retrosplenial circuits for allocentric-egocentric transformation of boundary coding. Elife *9*, e59816.

Winawer, J., Horiguchi, H., Sayres, R.A., Amano, K., and Wandell, B.A. (2010). Mapping hV4 and ventral occipital cortex: The venous eclipse. J. Vis. *10*, 1–1.

Zeki, S. (2003). Improbable areas in the visual brain. Trends Neurosci. *26*, 23–26.